







Mid-IR tunable CW and passively Q-switched laser operation of Dy-doped fluoride fiber

YUCHEN WANG,^{1,*}  TONEY T. FERNANDEZ,²  PINGHUA TANG,^{3,4}
NICOLA COLUCCELLI,⁴  STUART D. JACKSON,⁵ MARIO C.
FALCONI,⁶ FRANCESCO PRUDENZANO,⁶  PAOLO LAPORTA,^{1,4} AND
GIANLUCA GALZERANO¹ 

¹*Istituto di Fotonica e Nanotecnologie-CNR, Piazza Leonardo da Vinci 32, 20133 Milano, Italy*

²*MQ Photonics Research Centre, Department of Physics & Astronomy, Macquarie University, NSW, 2109, Australia*

³*School of Physics and Optoelectronics, Xiangtan University, Xiangtan 411105, China*

⁴*Dipartimento di Fisica-Politecnico di Milano, Piazza Leonardo da Vinci 32, 20133 Milano, Italy*

⁵*MQ Photonics, School of Engineering, Faculty of Science and Engineering, Macquarie University, North Ryde, NSW, Australia*

⁶*Department of Electrical and Information Engineering, Politecnico di Bari, 70125 Bari, Italy*

**yuchen.wang@polimi.it*

Abstract: We report a comprehensive characterization of tunable continuous-wave (CW) and passive Q-switching laser performance of Dy-doped zirconium fluoride fiber emitting around 3 μm . The in-band pumped CW laser operation is investigated for pump wavelengths varying from 2.7 μm to 2.825 μm , for fiber lengths ranging from 0.4 m to 2 m, and for output coupling efficiency from 10% to 50%, leading to a maximum laser slope efficiency of 44% and a tuning range larger than 300 nm. With Findlay-Clay analysis and Rigrod analyses, optimal cavity parameters are retrieved, paving the way for further optimizations in performance. The passively Q-switched laser operation of Dy-doped fluoride fiber is achieved employing a semiconductor saturable absorber mirror for the first time, demonstrating a stable operation with a minimum pulse duration of 580 ns, a highest repetition frequency of 103 kHz and a pulse energy up to 300 nJ.

© 2022 Optica Publishing Group under the terms of the [Optica Open Access Publishing Agreement](#)

1. Introduction

In the last decade, middle infrared (Mid-IR) lasers have attracted increasing attention and endeavors for their potential in diverse areas of fundamental science and industrial applications, including precision spectroscopy [1], trace-gas sensing [2], material processing [3] and medicine [4]. Compared to the visible and near-IR spectral regions, the mid-IR region from 3 to 15 μm is characterized by the presence of fundamental vibrational transitions of many inorganic and organic molecules, including notorious greenhouse gases and air pollutants [5], making mid-IR region of extreme interest for high-sensitivity spectroscopic investigations and quantitative analysis of agricultural and industrial wastes aiding in their reduction and recycling [6]. Moreover, when assisted by direct-comb spectroscopy and comb-assisted spectroscopy methods, mid-IR broadband and tunable lasers find also interesting applications in precision molecular spectroscopy and fundamental physics [7]. For these reasons, the development of coherent broad-band mid-IR laser sources, both in CW and pulsed regimes, is a technological cornerstone for not only fundamental science, but also for social and industrial innovation.

Extending the emission wavelength of high-performance laser sources further into the mid-IR spectral region is one of the frontiers of photonics research. Devices based on different working principles are under active investigation, both in tunable CW operation and pulsed operation regimes, including solid-state lasers [8], fiber lasers [9], quantum-cascade semiconductor lasers

[10] and optical parametric amplifiers and oscillators [11]. Compared to other technologies, fiber laser sources can be potentially more robust and compact, therefore suitable for more diverse application scenarios as already demonstrated in the last decades by near-IR Yb- and Er-doped silica fiber lasers.

Among the several rare-earth doped fibers suitable for mid-IR emission, the Dy-doped fluoride fiber shows great potentials for high-efficiency and broadband laser emission both in continuous-wave (CW) and pulsed regimes [12–14]. Characterized by a broad emission cross-section of nearly 300 nm in 3-dB bandwidth, Dy-based active medium promises a wider wavelength tuning range in CW and shorter pulses in mode-locked laser operation. In recent years, Dy-doped fluoride fiber lasers demonstrated CW operation emitting output powers higher than 10 W [15], slope efficiency reaching 91% [16], tuning range wider than 600 nm [17], and single-frequency operation with emission linewidth narrower than 100 kHz [18]. The pulsed laser operation is numerically studied [19] and demonstrated in gain-switching [20,21], Q-switching [22–24] and mode-locking regimes [25,26]. In particular, with the nonlinear pulse evolution mode-locking technique, the generation of sub-picosecond pulses has also been demonstrated [26]. Although several experimental demonstrations have been obtained with the Dy:ZBLAN fiber, a full characterization of this laser material has not been performed yet with specific attention to fiber propagation losses and optimum pump wavelength.

In this article, we present a comprehensive study on the laser performance of Dy-doped fluoride fiber in both continuous-wave and passive Q-switching regimes to better investigate the potential of this mid-IR laser source. The dependence of laser performance on several parameters including pump wavelength, fiber length, resonator configuration and output coupling has been investigated. With a semiconductor absorber mirror (SESAM), stable passive Q-switching operation has been achieved with repetition frequency up to 103 kHz and pulse energies reaching 300 nJ. In comparison to previous demonstrations of Dy-doped fluoride fiber laser switching based on different saturable absorption devices, the setup in this work provides the shortest pulse duration of 580 ns.

2. Characterization of Dy-doped fluoride fibers

The Dy-doped fluoride fibers (Le Verre Fluoré) used in this experiment has a glass composition based on zirconium fluoride (ZrF_4). The fiber structure has a step-index design with a core diameter of 12.5 μm , a cladding diameter of 125 μm and a numerical aperture of 0.16. The fiber core is doped with Dy^{3+} ions with a concentration of 0.2 mol% (or $3.63 \times 10^{25} \text{ m}^{-3}$). To characterize the absorption coefficient of the fiber, pump absorption measurements at the peak Dy absorption wavelength of 2.825 μm have been performed with the cutback technique at three different fiber lengths. The pump beam is steered by a couple of gold mirrors and coupled into the fiber using an aspheric lens with a focal length of 12.7 mm. The fiber is mounted on a steel groove placed on a precision five-axis stage to ensure high mechanical stability and fine alignment. The measured unabsorbed pump powers at the output of the active fiber for three fiber lengths of 34 cm, 63 cm and 93 cm are shown in Fig. 1(a). From these measurements both the coupling efficiency and the fiber absorption cross section can be retrieved. Indeed, the unabsorbed pump intensity at position z along the fiber I can be written in relation to the propagation distance z as:

$$\frac{dI}{dz} = - \left(\gamma_0 + \frac{\alpha_0}{1 + I/I_s} \right) I, \quad (1)$$

where α_0 is unsaturated absorption coefficient, γ_0 is the additional fiber loss not related to Dy-doping (0.01 dB/m) and I_s is the saturation intensity. This differential equation is solved numerically assuming an unsaturated absorption coefficient of 13.79 m^{-1} (–59.89 dB/m) in accordance with the nominal doping concentration. The saturation intensity is estimated to be $2.89 \times 10^8 \text{ W/m}^2$, considering an absorption cross-section of $3.8 \times 10^{-25} \text{ m}^2$ at 2825 nm, an upper

state lifetime of $0.632 \mu\text{s}$ [27], and an effective mode-field area of $165.7 \mu\text{m}^2$. The unabsorbed pump power at the end of the active fiber is calculated and shown in Fig. 1(a) as dashed lines for the three different fiber lengths. From the fitting results we retrieve a pump coupling efficiency η_c of 78%.

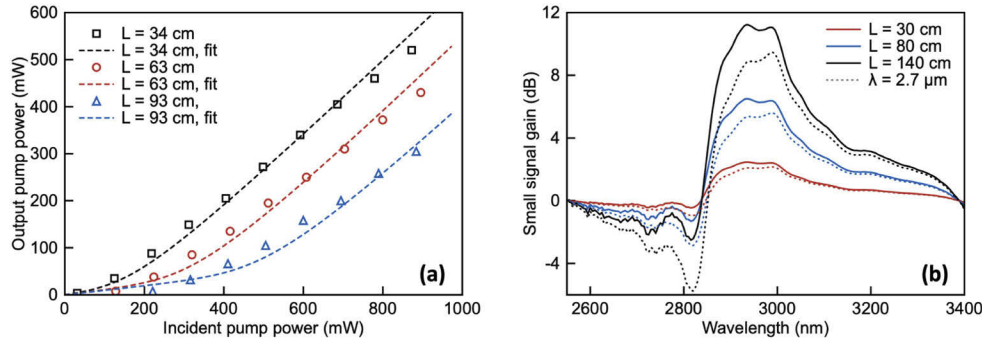


Fig. 1. (a) Measured residual pump power versus incident pump power at 2825 nm for fiber lengths of 34, 63 and 93 cm (with corresponding fitting curves shown in dashed lines) and (b) calculated unsaturated gain profile pumped at 2825 nm (2700 nm for the dashed lines) at 1 W of Dy-doped fluoride fibers with 30, 80 and 140 cm lengths.

Subsequently, using these parameters the unsaturated gain profiles of Dy-doped fluoride fibers with lengths of 30, 80 and 140 cm, at 2700 nm and 2825 nm pump wavelengths can be calculated [28], as shown in Fig. 1(b). Using a pump wavelength of 2700 nm, the maximum unsaturated gain is slightly lower compared to the pump wavelength of 2825 nm. At a pump power of 1 W, using a fiber length of 1.4 m, the small signal gain is larger than 10 dB at 3000 nm with a 3-dB bandwidth of approximately 150 nm.

3. Tunable CW laser performance

3.1. Experimental setup

The characterization of the CW laser performance is carried out with two different pump sources for the investigation of optimal pump wavelength. A home-made CW tunable $\text{Cr}^{2+}:\text{ZnSe}$ laser with output powers up to 2 W is used as a pump source between $2.65 \mu\text{m}$ and $2.75 \mu\text{m}$. An Er-doped fluoride fiber laser (LumIR) with output power up to 10 W is used for pumping at $2.825 \mu\text{m}$. Active fibers of different lengths have been used, ranging from 40 cm to 140 cm.

The CW laser resonator configurations used in the experiment are illustrated in Fig. 2. For the characterization of CW laser performance, linear laser resonators are implemented according to the pump sources and the laser operation regime. When the $\text{Cr}^{2+}:\text{ZnSe}$ laser is used as the pump source (see Fig. 2(a)), the polarization state of the pump beam is optimized by a half-wave plate (HWP) before it is reflected by a polarizing beam splitter (PBS). The PBS is implemented with 0.3-mm-thick Ge plate placed at Brewster's angle. For its high refractive index around 4 (for both pump and laser wavelengths), the s-polarized pump beam is reflected with a R (reflectance) $\sim 78\%$ while the p-polarized laser beam is transmitted with T (transmittance) $> 99\%$. The pump Gaussian beam is coupled to the fiber fundamental mode (LP_{01}) by an aspheric lens (Thorlabs AL72512-E) with a focal length of 12.7 mm. A dielectric high reflectivity (HR) mirror is butt-coupled to the other fiber tip to close the cavity together with the output coupler (OC). Three different partial reflectors are used as OCs in this experiment, with nominal reflectance of 50%, 80% and 90% at $2.94 \mu\text{m}$ (Layertec). When the Er-doped fluoride fiber laser is used as the pump source (see Fig. 2(b)), the PBS is substituted with a dichroic mirror (DM) with partial transmission at $2.825 \mu\text{m}$ ($T=41\%$) and high reflectivity at $3 \mu\text{m}$ ($R>99\%$).

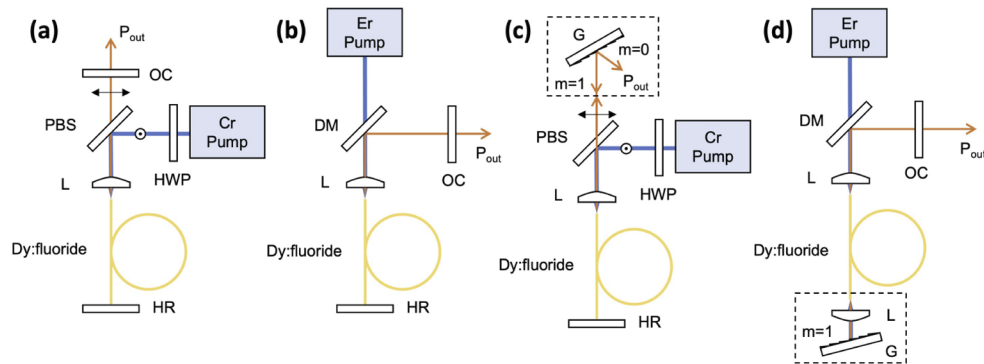


Fig. 2. Illustrative schematics of the resonator configurations: (a) laser resonator setup pumped with $\text{Cr}^{2+}:\text{ZnSe}$ laser, (b) laser resonator setup pumped with Er-doped fluoride fiber laser, (c) resonator setup with Littrow Type-I configuration for wavelength tuning (in dashed square) and (d) resonator setup with Littrow Type-II configuration for wavelength tuning (in dashed square). HWP, half-wave plate. PBS, polarizing beam splitter. DM, dichroic mirror. OC, output coupler. L, aspheric lens. HR, high-reflectivity dielectric mirror. G, blazed diffraction grating. P_{out} , output laser beam.

For the Dy laser wavelength tuning experiment, two different setups are adopted. For the setup with the $\text{Cr}^{2+}:\text{ZnSe}$ pump laser, a blazed diffraction grating (Richardson Gratings 53004BK01-736R) replaces the output coupler to close the cavity, forming a Type-I Littrow configuration. The zero-th order reflection of the grating is used as the output and the first-order diffraction is reflected back to form the resonator, as shown in Fig. 2(c). With the Er-doped fluoride fiber pump laser, a blazed diffraction grating and an aspheric lens are set in a Littrow configuration to replace the HR mirror for closing the cavity, as shown in Fig. 2(d). The pump power and the laser output power are measured with a thermopile power meter (Coherent LM-3). The output laser spectrum is characterized with a Fourier-transform infrared spectrometer (JASCO FT/IR-6000).

3.2. Results

With the $\text{Cr}^{2+}:\text{ZnSe}$ CW pump laser, the laser operation is first investigated using an active fiber with a length of 140 cm. The CW laser emission is first characterized for different output coupler transmittances (T_{OC}) at a fixed pump wavelength of $2.7 \mu\text{m}$ (Fig. 3(a)). With a T_{OC} of 50%, the threshold pump power (injected power) is around 188 mW. The laser operation remains stable when increasing the pump power up to 1 W, emitting up to 121 mW output power at $3.05 \mu\text{m}$ with a slope efficiency of roughly 17%. Reducing the T_{OC} to 20%, the threshold pump power remains unchanged, while the slope efficiency decreases to 10%. Further reducing the T_{OC} to 10%, the threshold decreases to about 100 mW and the slope efficiency reduces to 4.8%. At higher pump powers around 1 W, the saturation of output powers can be observed. Because of the clear saturation of laser output power, we have discarded the data with pump powers higher than 900 mW in the linear regression fitting. Under the free-running CW operation conditions, using a monochromator we observed that the laser emission wavelength varies from 2980 nm to 3050 nm. The emission of the CW free-running laser is multimode and its wavelength depends on the laser intracavity loss (alignment of the laser resonator), pump power and also the fiber length.

The same characterization is repeated for a fiber length of 47 cm (Fig. 3(b)). With the shorter fiber, the threshold pump power increased to around 390 mW. The slope efficiency almost doubled using the longer fiber, reaching 9%, 10.2% and 34% with output coupling efficiencies of 10%, 20% and 50%, respectively (here, we only used data with pump power lower than 700 mW for the linear fitting). However, the saturation of laser emission at higher pump powers is also more

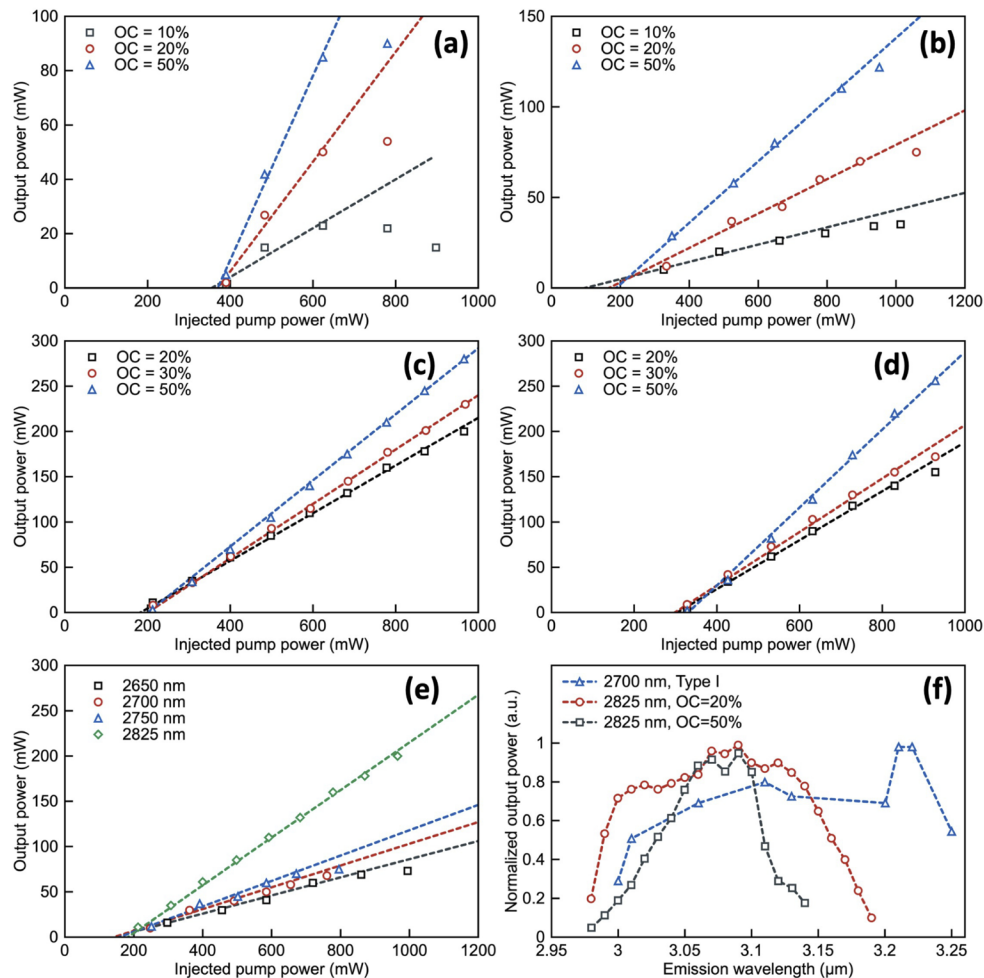


Fig. 3. CW laser performance characterization. Measurement results (symbols) and linear fittings (dashed lines) of laser output power versus injected pump power: (a) setup with a fiber length of 47 cm and pump wavelength of 2.7 μm , (b) setup with a fiber length of 140 cm and pump wavelength of 2.7 μm , (c) setup with a fiber length of 140 cm and pump wavelength of 2.825 μm , (d) setup with a fiber length of 200 cm and pump wavelength of 2.825 μm , (e) for the setup with a fiber length of 140 cm and pump wavelength varying from 2.65 μm to 2.825 μm with $T_{OC}=20\%$, (f) wavelength tuning curves using Littrow Type-I configuration at a pump wavelength of 2.7 μm and using Type-II configuration pumped at 2.825 μm .

prominent. For the case with $T_{OC}=10\%$, the output power starts to decrease for a pump power higher than 600 mW. The highest output power close to 90 mW is reached with $T_{OC}=50\%$ at a pump power of 800 mW.

Then the effect of different pump wavelengths on the laser performance is investigated with a 140-cm-long fiber and a $T_{OC}=20\%$ (Fig. 3(e)). With increasing pump wavelengths of 2.65 μm , 2.7 μm , 2.75 μm to 2.825 μm , the laser slope efficiency using a 20%-OC increases from 10%, 12%, 14% to 26.3%, respectively. The dependence of the slope efficiency on the pump wavelength reflects the increasing pump absorption cross-section in this wavelength region [27]. When pumped by the $\text{Cr}^{2+}:\text{ZnSe}$ laser, the threshold pump power is around 167 mW, similar to

the results obtained when varying the output coupler transmittance. The threshold pump power is around 182 mW using the pump laser at 2.825 μm , which might be due to slightly higher intracavity losses in the different setup configuration. Further increasing the fiber length to 2 m, a higher slope efficiency reaching 44% is achieved with a OC of 50% and a pump wavelength of 2825 nm (Fig. 3(d)). From these results, we experimentally observe that the highest laser efficiency with respect to the pump wavelength can be achieved at 2825 μm , which is closer to the peak of absorption of Dy^{3+} ions.

Along with the comprehensive characterization of laser performance with different fiber lengths, we also performed a laser loss analysis analogous to the Findlay-Clay analysis [29]. The laser slope efficiency η can be expressed as $\eta = \eta_0 \gamma_2 / (\gamma_1 + \gamma_2 + 2\gamma_i)$, where η_0 is the maximum laser efficiency, γ_1 is the logarithmic reflectivity to the HR mirror (thus $\gamma_1 \approx 0$), γ_2 is the logarithmic output coupling ratio, and γ_i is the logarithmic single-pass intracavity loss [30]. By fitting the slope efficiencies obtained with different output coupling percentage to this analytical model, for the 2-m-long fiber, we obtain a maximum efficiency of 52.8% and a total single-pass logarithmic loss γ_i of 0.45. For the 1.4-m-long fiber, the maximum efficiency is calculated to be 46% with an total single-pass intracavity loss γ_i of 0.38. In the resonator configuration employed in this experiment, the known fixed intracavity losses include the coupling efficiency at the laser wavelength, the imperfect coating of the aspheric lens and the dichroic mirror. From these data of two different fiber lengths, we can retrieve a propagation loss depending on the fiber length of 0.12 dB/m (higher than the nominal fiber losses according to the fiber supplier for single-mode fiber of 0.025 dB/m) and a fixed single-pass logarithmic loss term of 0.22 dB (a percentage loss of around 4.8%).

From these results, we also performed the Rigrod analysis to retrieve the optimum output coupling ratio [31]. From the expression for the threshold pump power:

$$P_{th} = P_{thm} \frac{\gamma_i + \frac{\gamma_1}{2} + \frac{\gamma_2}{2}}{\gamma_i + \frac{\gamma_1}{2}}, \quad (2)$$

where P_{th} is the threshold pump power, P_{thm} is the minimum threshold pump power (for a output coupling of 0%), we can obtain the minimum threshold pump power for the 2-m-long fiber resonator to be 149 mW (83.3 mW for the 1.4-m-long fiber resonator). The optimum output coupling ratio S_{opt} be expressed as [30]

$$S_{opt} = \frac{\frac{\gamma_2}{2}}{\gamma_i + \frac{\gamma_1}{2}} = \sqrt{\frac{P_p}{P_{thm}}} - 1 \quad (3)$$

which is the value of S that maximizes the expression for the laser output power:

$$P_{out} = \left[A_b I_s \left(\gamma_i + \frac{\gamma_1}{2} \right) \right] S \left[\left(\frac{P_{th}/P_{thm}}{S+1} \right) - 1 \right]. \quad (4)$$

Considering a pump power 10 times of the minimum threshold pump power, we find $S_{opt} = 2.16$, which gives an optimum output coupling for the 2-m-long fiber laser of $T_{OC} = 64\%$ (which means an mirror reflectivity $R_{OC} = 36\%$). The same procedure for the 1.4 m fiber leads to an optimum output coupling of $T_{OC} = 69\%$ ($R_{OC} = 31\%$). From these results the laser performance can be further improved by employing the optimal output coupling ratio, to achieve a slope efficiency near to the theoretical maximum of 53.8%, using the same experimental setup.

The continuous tuning of laser emission wavelength is investigated by replacing either the output coupler or the HR mirror with a diffraction grating in type-I or type-II Littrow configurations, as shown in Fig. 2(c) and (d). The type-II Littrow configuration introduces higher losses into the resonator because of the imperfect coupling of back-reflected beam with the fiber. As a result,

with type-I Littrow configuration, a broader tuning range can be achieved from 3 μm to 3.25 μm , covering a range of 250 nm (Fig. 3(d)), limited on the longer wavelength edge most likely by the performance of the diffraction grating. While with Type-II configuration the range of tunability is limited to about 190 nm, from 2.98 μm to 3.19 μm , limited most probably by the higher intracavity losses due to the addition of extra components in stead of the butt-coupled HR mirror. Although the achieved tuning range is narrower than previously reported demonstration of tunable laser emission mainly because of the limited range of operation of cavity components and higher intracavity losses, we can conclude that a Littrow Type-I configuration is comparatively favorable for achieving broader tuning range, at the cost of an varying output beam path.

4. Passive Q-switching laser performance

4.1. Experimental setup

To achieve passively Q-switched operation of the Dy-doped fluoride fiber laser, the CW resonator setup is modified to incorporate the semiconductor saturable absorber mirror (SESAM) in the laser cavity (as shown in Fig. 4). The SESAM (Batop) has a designed working wavelength of 3000 nm, an absorbance of 33%, a modulation depth of 18%, a saturation fluence of 70 $\mu\text{J}/\text{cm}^2$, a relaxation time constant of 10 ps and a non-saturable loss of 15%.

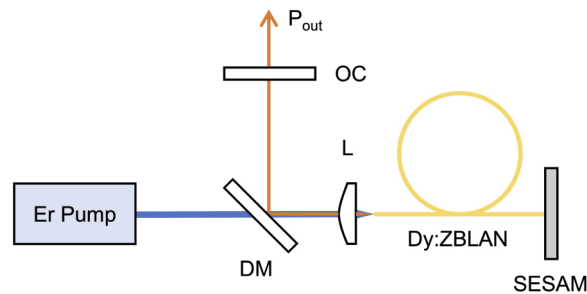


Fig. 4. Passive Q-switching resonator setup with SESAM. DM, dichroic mirror. OC, output coupler. L, aspheric lens. P_{out} , output laser beam.

The linear resonator design is relatively simple and compact. The Er-doped fluoride fiber pump laser is transmitted through a dichroic mirror and coupled into the 1.4-m long Dy-doped fiber by an aspheric lens. The SESAM is butt-coupled to the other end of the fiber to enclose the cavity, reflecting back the fundamental mode of the fiber. The relatively small mode field diameter of 15.2 μm ($1/e^2$ intensity level at 3 μm) ensures a sufficient peak power for the saturation of the SESAM. The dichroic mirror reflects the laser beam towards the 20% output coupler which closes the cavity.

4.2. Results

Figure 5 summarizes the performance of the Dy:ZBLAN laser in passive Q-switching operation as a function of the pump power in terms of average output power, pulse energy, pulse repetition rate, and pulse duration. The Q-switched operation has a threshold pump power around 420 mW and a slope efficiency of around 9.7%. The maximum average output power reaches 30 mW for 700 mW pump power. The output pulse train is monitored by a liquid nitrogen cooled amplified HgCdTe photodetector (Kolmar Technologies) with 200 MHz bandwidth. The photodetector signal is then sent to an oscilloscope to monitor the pulse shape and to a radio-frequency electrical spectrum analyzer (ESA) to measure the repetition frequency. The dependence of pulse repetition frequency and pulse duration on the pump power is shown in Fig. 5(b). With

increasing pump power, the pulse duration decreases until nearly saturates to the minimum value of 580 ns whereas the pulse repetition increase from the minimum value of 37 to 103 kHz.

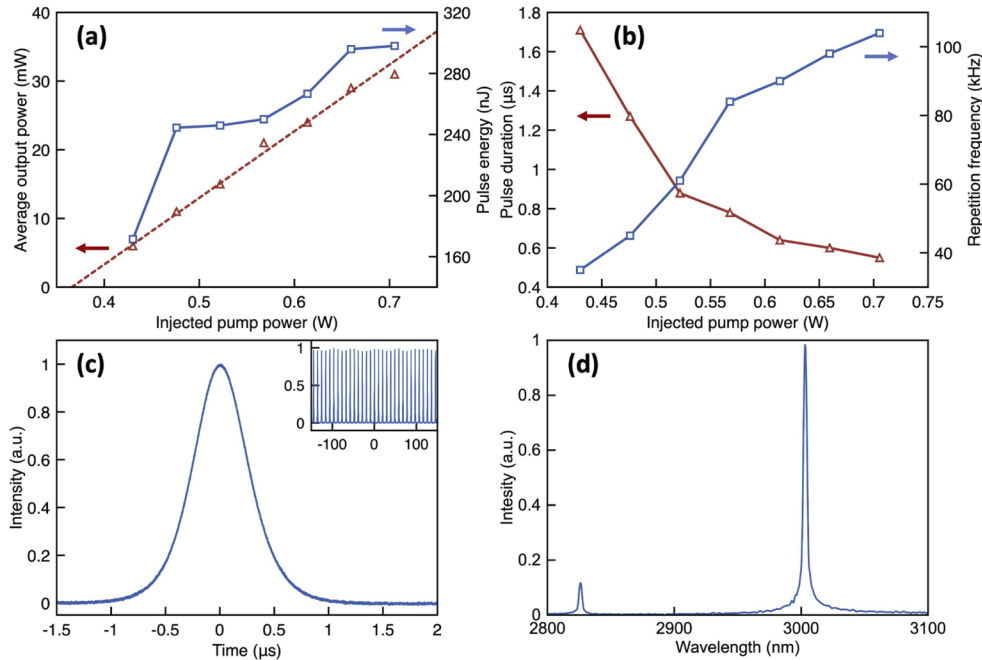


Fig. 5. Q-switched laser performance: (a) Measured average output power (red) and pulse energy (blue) as a function of the pump power, and (b) the measured pulse duration (red) and repetition frequency (blue) as functions of the pump power. Characterization of passively Q-switched pulse train: (c) the oscilloscope trace of a single Q-switched pulse of 580 ns duration (inset: the stability of Q-switched pulse train, (d) the corresponding optical spectrum measured by an Fourier-transform infrared spectrometer (resolution bandwidth 0.3 nm)

A single pulse trace with a full width at half maximum (FWHM) duration of 580 ns is shown in Fig. 5(c). The pulse train shows a good intensity stability, as shown in the inset of the same figure. The output beam is then sent to a Fourier-transform infrared spectrometer to measure its optical spectrum which is shown in Fig. 5(d). The optical spectrum of the Q-switched pulses at 700 mW pump power is centered at 3003 nm, with a full-width at half maximum (FWHM) of 3.6 nm. At this pump level, the pulse repetition frequency spectrum measured by the ESA shows a single peak at 103.4 kHz with a signal-to-noise ratio of 36 dB, indicating a high operation stability and low timing jitter. Taking into account the measured pulse duration and repetition frequency at different pump powers, the pulse energy can be calculated (shown in Fig. 5(a)). At a pump power of 700 mW, the pulse energy reaches 300 nJ.

In Table 1, recent results of passively Q-switched Dy-, Er- and Ho-doped fluoride fiber lasers emitting at 3 μm are listed. In comparison to previous demonstrations with Dy- and Ho-doped fluoride fiber at 3 μm, the setup in this work provides the shortest pulse duration of 580 ns even at a moderate pulse energy level. Demonstrations of Q-switching based on Er-doped fibers show better performance in terms of pulse duration and repetition rate, but their emission wavelength is limited to around 2.8 μm. Compared to the nanomaterials used in several other works, SESAMs have advantages in their mature fabrication technologies and excellent long-term stability. We believe that following our demonstration of Q-switching with SESAM for Dy-doped fluoride fiber lasers, with further optimizations in efficiency and power scaling with all-fiber resonator

designs, stable and high-performance passively Q-switched fiber laser sources at 3 μm should be on the verge of reaching industrial applications.

Table 1. Summary of recent demonstrations of passively Q-switched fiber lasers emitting around 3 μm . SA, saturable absorber. λ , emission center wavelength. f_R , pulse repetition frequency. τ_p , pulse duration. E_p , pulse energy. BP, black phosphorus.

Active element	SA	λ (μm)	f_R (kHz)	τ_p (μs)	E_p (μJ)	Reference
Er^{3+}	Fe_3O_4	2.8	161	0.37	2.0	[32]
Er^{3+}	SESAM	2.79	146.3	0.31	6.9	[33]
Ho^{3+}	SESAM	2.979	47.6	1.68	6.65	[34]
Ho^{3+}	Bi_2Te_3	2.979	81.96	1.37	3.99	[35]
Dy^{3+}	PbS	2.71–3.08	166.8	0.795	1.51	[22]
Dy^{3+}	Fe_3O_4	2.81–3.03	123	1.25	0.9	[23]
Dy^{3+}	BP	3.04	86	0.74	1.0	[24]
Dy^{3+}	SESAM	3.0	103	0.58	0.3	This Work

5. Conclusions

In conclusion, we have reported a comprehensive and systematic characterization of the tunable CW and passive Q-switching laser performance of Dy-doped zirconium fluoride fibers. Using different fiber lengths, output coupling efficiencies and pump wavelengths we have reached a laser slope efficiency of 44% which is limited by the intracavity losses as compared to the reported all-fiber resonators. The passive Q-switching of Dy-doped fluoride fiber laser is demonstrated with a SESAM for the first time, to the best of our knowledge, providing pulses with minimum duration of 580 ns, highest peak power of 0.52 W, pulse energy up to 300 nJ and repetition frequency of 103 kHz. These experimental results form a direct comparison of laser performances among different cavity configurations, providing insights for further improvement of Dy-doped fluoride fiber laser design in terms of pump wavelength, fiber length and output coupling ratio, that can be of significant value also for the generation of femtosecond pulses and the synthesis of optical frequency combs in the mid-IR spectral region around 3 μm .

Funding. Extreme Light Infrastructure Nuclear Physics ; Ministero dell'Istruzione, dell'Università e della Ricerca; China Scholarship Council (202008430040).

Acknowledgments. P. Tang thanks the China Scholarship Council and Politecnico di Milano for his 1-year scholarship and visiting professor fellowship, respectively.

Disclosures. The authors declare no conflicts of interest.

Data availability. Data underlying the results presented in this paper are not publicly available at this time but may be obtained from the authors upon reasonable request.

References

1. A. Gambetta, E. Vicentini, Y. Wang, N. Coluccelli, E. Fasci, L. Gianfrani, A. Castrillo, V. Di Sarno, L. Santamaria, P. Maddaloni, P. De Natale, P. Laporta, and G. Galzerano, "Absolute frequency measurements of chf 3 doppler-free ro-vibrational transitions at 8.6 μm ," *Opt. Lett.* **42**(10), 1911–1914 (2017).
2. L. Nugent-Glandorf, F. R. Giorgetta, and S. A. Diddams, "Open-air, broad-bandwidth trace gas sensing with a mid-infrared optical frequency comb," *Appl. Phys. B* **119**(2), 327–338 (2015).
3. C. Frayssinous, V. Fortin, J.-P. Bérubé, A. Fraser, and R. Vallée, "Resonant polymer ablation using a compact 3.44 μm fiber laser," *J. Mater. Process. Technol.* **252**, 813–820 (2018).
4. A. B. Seddon, "Mid-infrared (IR)—a hot topic: The potential for using mid-ir light for non-invasive early detection of skin cancer in vivo," *Phys. Status Solidi B* **250**(5), 1020–1027 (2013).
5. G. B. Rieker, F. R. Giorgetta, W. C. Swann, J. Kofler, A. M. Zolot, L. C. Sinclair, E. Baumann, C. Cromer, G. Petron, C. Sweeney, P. P. Tans, I. Coddington, and N. R. Newbury, "Frequency-comb-based remote sensing of greenhouse gases over kilometer air paths," *Optica* **1**(5), 290–298 (2014).

6. D. I. Herman, C. Weerasekara, L. C. Hutcherson, F. R. Giorgetta, K. C. Cossel, E. M. Waxman, G. M. Colacion, N. R. Newbury, S. M. Welch, B. D. DePaola, I. Coddington, E. A. Santos, and B. R. Washburn, "Precise multispecies agricultural gas flux determined using broadband open-path dual-comb spectroscopy," *Sci. Adv.* **7**(14), 1 (2021).
7. N. Picqué and T. W. Hänsch, "Frequency comb spectroscopy," *Nat. Photonics* **13**(3), 146–157 (2019).
8. S. B. Mirov, I. S. Moskalev, S. Vasilyev, V. Smolski, V. V. Fedorov, D. Martyshev, J. Peppers, M. Mirov, A. Dergachev, and V. Gapontsev, "Frontiers of mid-ir lasers based on transition metal doped chalcogenides," *IEEE J. Sel. Top. Quantum Electron.* **24**(5), 1–29 (2018).
9. S. D. Jackson and R. Jain, "Fiber-based sources of coherent mid-ir radiation: key advances and future prospects," *Opt. Express* **28**(21), 30964–31019 (2020).
10. F. Capasso, "High-performance midinfrared quantum cascade lasers," *Opt. Eng.* **49**(11), 111102 (2010).
11. N. Leindecker, A. Marandi, R. L. Byer, K. L. Vodopyanov, J. Jiang, I. Hartl, M. Fermann, and P. G. Schunemann, "Octave-spanning ultrafast opo with 2.6–6.1 μm instantaneous bandwidth pumped by femtosecond tm-fiber laser," *Opt. Express* **20**(7), 7046–7053 (2012).
12. M. R. Majewski, R. I. Woodward, and S. D. Jackson, "Dysprosium mid-infrared lasers: current status and future prospects," *Laser Photonics Rev.* **14**(3), 1900195 (2020).
13. Z. Wang, B. Zhang, J. Liu, Y. Song, and H. Zhang, "Recent developments in mid-infrared fiber lasers: Status and challenges," *Opt. Laser Technol.* **132**, 106497 (2020).
14. X. Zhu, G. Zhu, C. Wei, L. V. Kotov, J. Wang, M. Tong, R. A. Norwood, and N. Peyghambarian, "Pulsed fluoride fiber lasers at 3 μm ," *J. Opt. Soc. Am. B* **34**(3), A15–A28 (2017).
15. V. Fortin, F. Jobin, M. Larose, M. Bernier, and R. Vallée, "10-w-level monolithic dysprosium-doped fiber laser at 3.24 μm ," *Opt. Lett.* **44**(3), 491–494 (2019).
16. M. R. Majewski, M. Z. Amin, T. Berthelot, and S. D. Jackson, "Directly diode-pumped mid-infrared dysprosium fiber laser," *Opt. Lett.* **44**(22), 5549–5552 (2019).
17. M. R. Majewski, R. I. Woodward, and S. D. Jackson, "Dysprosium-doped zblan fiber laser tunable from 2.8 μm to 3.4 μm , pumped at 1.7 μm ," *Opt. Lett.* **43**(5), 971–974 (2018).
18. P. Tang, Y. Wang, E. Vicentini, N. Coluccelli, P. Laporta, and G. Galzerano, "Single-frequency dy:zblan fiber laser tunable in the wavelength range from 2.925 to 3.250 μm ," *Journal of Lightwave Technology under review*, 00 (2021).
19. M. C. Falconi, D. Laneve, M. Bozzetti, T. T. Fernandez, G. Galzerano, and F. Prudenzeno, "Design of an efficient pulsed Dy³⁺: ZBLAN fiber laser operating in gain switching regime," *J. Lightwave Technol.* **36**(23), 5327–5333 (2018).
20. H. Luo, Y. Xu, J. Li, and Y. Liu, "Gain-switched dysprosium fiber laser tunable from 2.8 to 3.1 μm ," *Opt. Express* **27**(19), 27151–27158 (2019).
21. L. Pajewski, L. Sójka, S. Lamrini, T. M. Benson, A. B. Seddon, and S. Sujecki, "Gain-switched Dy³⁺: ZBLAN fiber laser operating around 3 μm ," *Journal of Physics: Photonics* **2**, 014003 (2019).
22. H. Luo, J. Li, Y. Gao, Y. Xu, X. Li, and Y. Liu, "Tunable passively Q-switched dy³⁺-doped fiber laser from 2.71 to 3.08 μm using pbs nanoparticles," *Opt. Lett.* **44**(9), 2322–2325 (2019).
23. J. Yang, J. Hu, H. Luo, J. Li, J. Liu, X. Li, and Y. Liu, "Fe₃O₄ nanoparticles as a saturable absorber for a tunable Q-switched dysprosium laser around 3 μm ," *Photonics Res.* **8**(1), 70–77 (2020).
24. R. Woodward, M. Majewski, N. Macadam, G. Hu, T. Albrow-Owen, T. Hasan, and S. Jackson, "Q-switched Dy: ZBLAN fiber lasers beyond 3 μm : comparison of pulse generation using acousto-optic modulation and inkjet-printed black phosphorus," *Opt. Express* **27**(10), 15032–15045 (2019).
25. R. Woodward, M. Majewski, and S. Jackson, "Mode-locked dysprosium fiber laser: Picosecond pulse generation from 2.97 to 3.30 μm ," *APL Photonics* **3**(11), 116106 (2018).
26. Y. Wang, F. Jobin, S. Duval, V. Fortin, P. Laporta, M. Bernier, G. Galzerano, and R. Vallée, "Ultrafast Dy³⁺: fluoride fiber laser beyond 3 μm ," *Opt. Lett.* **44**(2), 395–398 (2019).
27. L. Gomes, A. F. H. Librantz, and S. D. Jackson, "Energy level decay and excited state absorption processes in dysprosium-doped fluoride glass," *J. Appl. Phys.* **107**(5), 053103 (2010).
28. H. Pask, R. J. Carman, D. C. Hanna, A. C. Tropper, C. J. Mackechnie, P. R. Barber, and J. M. Dawes, "Ytterbium-doped silica fiber lasers: versatile sources for the 1–1.2/spl μm region," *IEEE J. Sel. Top. Quantum Electron.* **1**(1), 2–13 (1995).
29. H. Zhao and A. Major, "Dynamic characterization of intracavity losses in broadband quasi-three-level lasers," *Opt. Express* **22**(22), 26651–26658 (2014).
30. O. Svelto, *Principles of Lasers* (Springer, 1998).
31. W. W. Rigrod, "Saturation effects in high-gain lasers," *J. Appl. Phys.* **36**(8), 2487–2490 (1965).
32. C. Wei, X. Zhu, R. A. Norwood, and N. Peyghambarian, "Passively Q-switched 2.8- μm nanosecond fiber laser," *IEEE Photonics Technol. Lett.* **24**(19), 1741–1744 (2012).
33. Y. Shen, Y. Wang, K. Luan, K. Huang, M. Tao, H. Chen, A. Yi, G. Feng, and J. Si, "Watt-level passively Q-switched heavily Er³⁺-doped ZBLAN fiber laser with a semiconductor saturable absorber mirror," *Sci. Rep.* **6**(1), 1–7 (2016).
34. J. Li, H. Luo, Y. He, Y. Liu, L. Zhang, K. Zhou, A. Rozhin, and S. Turystyn, "Semiconductor saturable absorber mirror passively Q-switched 2.97 μm fluoride fiber laser," *Laser Phys. Lett.* **11**(6), 065102 (2014).
35. J. Li, H. Luo, L. Wang, C. Zhao, H. Zhang, H. Li, and Y. Liu, "3- μm mid-infrared pulse generation using topological insulator as the saturable absorber," *Opt. Lett.* **40**(15), 3659–3662 (2015).